Article

Effects of Electrode Negative Pulsing Ratio in Direct Energy Deposition via Variable-Polarity Cold Metal Transfer Process on the Deposition Behavior and Microstructural Characteristics

Tae Hyun Lee [1,2], Cheolhee Kim [1,3] and Minjung Kang [1,*]

1   Advanced Joining & Additive Manufacturing R&D Department, Korea Institute of Industrial Technology, Incheon 21999, Korea; dlxogus31@kitech.re.kr (T.H.L.); chkim@kitech.re.kr (C.K.)
2   Department of Mechanical Design Engineering, Hanyang University, Seoul 04763, Korea
3   Department of Mechanical and Materials Engineering, Portland State University, Portland, OR 97207, USA
*   Correspondence: kmj1415@kitech.re.kr

Abstract: Interest in research on the application of variable-polarity cold metal transfer mode in wire-based direct energy deposition has been growing; particularly popular are investigations into the respective influences of polarity, amplitude of the arc current, and polarity variation sequence on the quality of the final product manufactured via additive manufacturing. The application of the electrode-negative phase is more capable of yielding relatively large droplets and increasing the weight of the deposited material. However, the proportions of the electrode positive phase are typically larger than those of the electrode-negative phase because it maintains arc stability and droplet transfer. This discrepancy has prevented the accurate evaluation of the effects of the polarity mode and polarity sequences on the deposition characteristics associated with variable-polarity cold metal transfer. In this study, variable-polarity cold metal transfer was performed using a tuned waveform, and the effects of the electrode-negative pulsing ratio and pulse repetition on the geometrical features and deposition rate were assessed. The weight tended to increase with decreasing welding speed and increasing electrode-negative pulsing ratio. The number of repetitions influenced molten pool behavior, and when sufficiently high, induced ripple formation via droplet accumulation below the electrode. In addition, the effects of the electrode-negative pulsing ratio and repetition on the microstructure formation were analyzed. It was revealed that the average grain size was related to the amount of supplied energy and polarity switching during grain formation.

Keywords: variable-polarity cold metal transfer; electrode-negative pulsing ratio; repetition; droplet transfer; molten pool behavior; microstructure

1. Introduction

Additive manufacturing (AM) is a promising alternative for fabricating extremely high buy-to-fly ratio components with complex geometry [1]. Generally, the deposition rate of laser or electron beam deposition is in the order of 2–10 g/min [2–4], compared with 50–130 g/min for arc welding-based AM technology [5–7]. For that reason, wire arc additive manufacturing (WAAM) using an arc heat source is a promising technology for manufacturing with medium to large size in terms of productivity, cost-competitiveness, and energy efficiency [1,7–9]. Especially, WAAM typically entails the use of gas metal arc welding (GMAW), plasma arc welding, and gas tungsten arc welding (GTAW) power sources to build parts using a layer-by-layer approach. Among the WAAM arc welding processes, GMAW entails the utilization of a coaxially fed wire and an arc between the end of the wire and the base metal; this setup enables high energy efficiency because anode and cathode heating facilitate the melting of the wire and base metal. GMAW power supplies are designed for constant current, constant voltage, or pulsed current with an electrode-positive (EP) polarity; an electrode-negative (EN) polarity; or a variable-polarity

(VP) design. Among them, VP-GMAW are currently rarely applied in industry because their mechanisms and characteristics have yet to be fully elucidated [10].

Nonetheless, the application of the EN phase has the benefits of providing good gap-bridging ability and high wire-melting efficiency regardless of the metal droplet transfer characteristics. The wire melting rate associated with GMAW can be expressed as a quadratic function of the average welding current. Hu et al. [11] verified that, as compared to the constant voltage EP-GMAW process with the same average welding current, a higher wire melting rate could be achieved via the VP-GMAW process by selecting proper heat inputs for the EN and EP periods. This indicates that the VP-GMAW process can increase WAAM deposition efficiency. Kiran et al. [12] insisted that the application of the EN phase helps to reduce welding defects such as burn through, underfill, and distortion in sheet metal welding. Wang et al. [13] built WAAM parts using a VP-GTAW heat source with 4043 and 5356 filler wires; they discussed the effects of the ratio of the electrode-positive/negative cycles on the microstructure–strength relationship. Harwig et al. [14] evaluated VP-GMAW processes and reported that the current waveform strongly influenced the arc concentration and droplet behavior. They revealed that the electrode tip covered by the EN arc melted rapidly; this consequently contributed to increase the droplet volume growth rate. Klein and Schnall [10] also demonstrated that, in VP-GMAW processes, the polarity and repetition rate of an arc can alter the heat input to the base metal, as well as its cooling rate. The ratio of the EN phase duration to the entire period, which is called the EN ratio, influenced the wire melting rates and droplet sizes, as well as the heat input and cooling rate. It is well-known that the EP polarity helps to maintain the stability of arc and droplet transfer, whereas the EN polarity increases the wire melting rate and reduces the heat input to the base metal [12,15]. However, GMAW processes with EN and VP modes have been conducted under a very limited range of parameters because of the arc and droplet transfer instabilities.

A VP-GMAW process that incorporates reciprocating wire feeding and short-circuit metal transfer, i.e., cold metal transfer (CMT), was introduced as a VP-CMT process; the automatic short-circuit detection and mechanically controlled wire feeding in the process were demonstrated to eliminate arc and droplet transfer instabilities. Specifically, the electrode wire moved forward and backward at a high frequency (up to 130 Hz) during welding, and the enhanced process stability afforded low heat input and nearly zero spatters. Recently, several research papers have been published on VP-CMT welding. Su et al. [16] evaluated the effects of heat input on the microstructure and mechanical properties of Mg alloys fabricated via WAAM. Cong et al. analyzed the porosity distribution in Al–Cu alloy welds manufactured via variant CMT processes such as CMT, CMT advanced, CMT pulse, and CMT pulse advanced processes [17,18]. The geometrical features [19] and microstructures [18] were also assessed. They mentioned that the porosity and microstructural anisotropy were successfully reduced in the VP-CMT process. Owing to such reports, the amount of WAAM-related research focused on the VP-CMT mode has been increasing; particularly, the number of investigations into the respective influences of polarity, the amplitude of the arc current, and the polarity variation sequence [10] on the quality of the final product manufactured via AM have been increasing. However, the results of previous studies have demonstrated asymmetry in the current and voltage profiles between the EP and EN modes. This means that the heat input per EP mode pulse was different from that per EN mode pulse because the EP and EN mode pulses had different peak values and periods. This discrepancy prevented the accurate evaluation of the effects of the polarity mode and polarity sequences on the deposition characteristics.

In this study, the peak current, detach current, and base currents in the EP and EN mode pulses were finely tuned; additionally, the symmetric pulses during both polarity phases were implemented in VP-CMT processes. An Al–Mg alloy was deposited via VP-CMT. The drop transfer and arc stability, deposition characteristics, and microstructures were evaluated according to the polarity arrangement.

2. Experimental Setup

The automated welding system consisted of a VP-GMAW (Fronius, CMT 4000 Advanced, Wels, Austria) power source to induce polarity change, a wire feeding system, and a 6-axis robot manipulator. The dimensions of the Al 5083 substrate were 300 mm × 120 mm × 16 mm. The substrate was scrubbed with sandpaper and washed with ethanol to eliminate any remnants of oxide or grease prior to WAAM being applied. WAAM was applied with a working angle of 0°, and the contact tip-to-workpiece distance was set to 15 mm, as shown in Figure 1. An Al 5183 filler wire with a diameter of 1.2 mm was used, and the chemical compositions of the used materials (i.e., substrate and filler wire) are given in Table 1. High-purity argon (99.9%) was supplied as a shielding gas at a flow rate of 20 L/min. The welding conditions and parameter details are listed in Table 2.
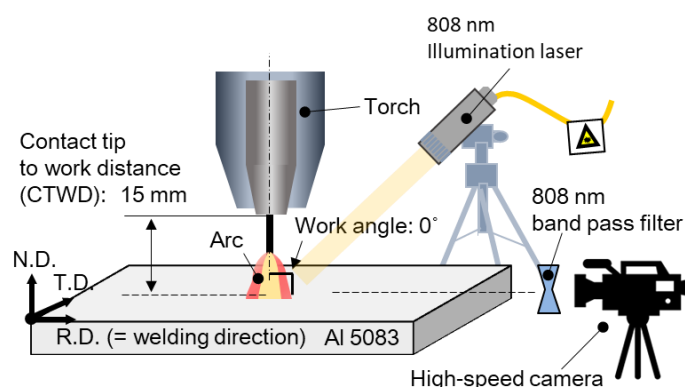
Figure 1. Experimental setup applied in experiment.

Table 1. Chemical composition of the substrate and filler wire.

| Materials	Chemical Composition (wt.%)						
	Si	Mn	Cr	Cu	Zn	Mg	Fe
Al 5083, 16 mm (substrate)	0.40	0.4–1.0	0.05–0.25	0.1	0.25	4.0–4.9	0.4
Al 5183, 1.2 mm (filler wire)	0.40	0.5-1.0	0.05–0.25	0.02	0.25	4.3–5.2	0.4

Table 2. Welding conditions and levels applied in the welding stage of the VP-GMAW process.

Variable	Parameter (Level)
Welding speed (m/min)	0.3, 0.5, 0.7 (3 levels)
EN pulsing ratio	0, 0.1, 0.25, 0.33, 0.5, 0.67, 0.75, 0.9, 1 (9 levels)
Repetition	1, 3, 5 (3 levels)

The polarity change [20–22] and pulse repetition [10] are known to determine the surface quality and heat distribution of the deposited material. To assess the effects of waveforms on the deposited material and metallurgical features, the magnitudes of the currents were artificially matched for the peak, detach, and base periods. A schematic diagram and the parameters of the applied waveform are respectively presented in Figure 2 and Table 3. In this study, the one-cycle fraction of the EN pulse was defined as the R_{EN}, while the minimum number of pulses with the same polarity in one-cycle was described as the repetition Equation (1). When the numbers of the EP and EN pulsing cycles were 2:1 and 6:3, both cycles had the same EN pulsing ratio of 0.33; however, the repetitions were 1

and 3, respectively. Therefore, the phase change frequency was three times higher in the 2:1 case, as shown in Figure 3.

$$\text{EN pulsing ratio}(R_{EN}) = \frac{\text{Number of EN pulse in a cycle}}{\text{Total number of pulse in a cycle}} \tag{1}$$
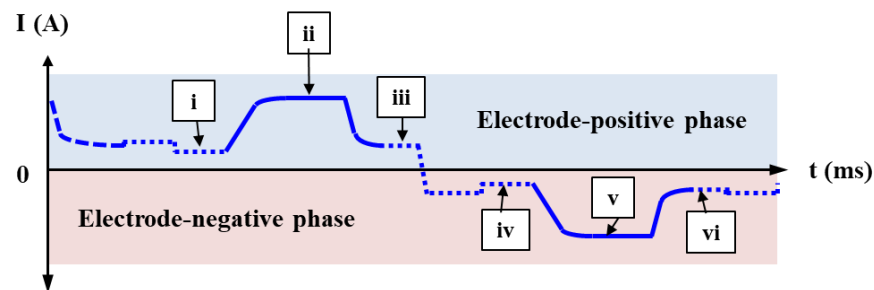
Figure 2. Schematic of current waveform used in the experiment.

Table 3. Current parameters applied to yield the results shown in Figure 3.

Sub-Phase	Concept	Value
i	Base current in EP pulse phase (IB_EP)	80 A
ii	Peak current in EP pulse phase (IP_EP)	244 A
iii	Detach current in EP pulse phase (ID_EP)	96 A
iv	Base current in EN pulse phase (IB_EN)	80 A
v	Peak current in EN pulse phase (IP_EN)	244 A
vi	Detach current in EN pulse phase (ID_EN)	96 A
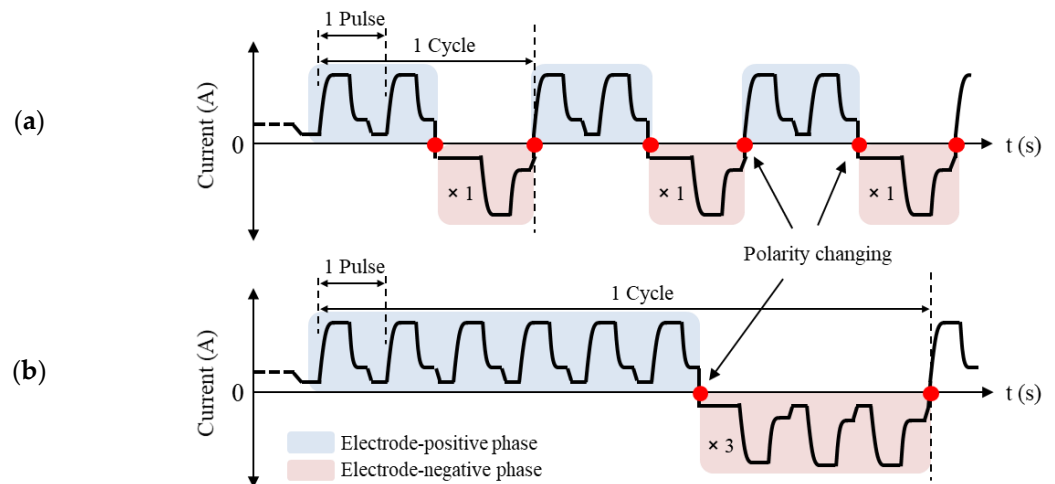
Figure 3. Current waveform schemes associated with an EN pulsing ratio of 0.33, with variable repetition in (**a**) one and (**b**) three times.

The current and voltage waveforms were measured by using a data acquisition system (NI 9229 module, National Instruments, Austin, TX, USA) with a sampling frequency of 50 kHz. The molten pool was observed via a high-speed camera (UX50, Photron, San Diego, CA, USA) with a diode laser illumination. The high-speed camera was applied at an angle of 0° relative to the specimen. Color and mono images were recorded at a frame rate of 5000 frames per second. An illumination laser (LIMO, Dortmund, Germany) with wavelength of 808 nm and maximum power of 120 W was employed. A bandpass filter (Edmund optics, Barrington, NJ, USA) transmitting radiation within 808 nm ± 1.5 nm was used. After the welding, the weld bead appearance was photographed to evaluate the weld bead consistency. The cross-sectional images prepared to analyze the substrate

dilution, penetration, and microstructural components. These specimens were polished and etched with a solution comprising 1 mL of HF, 1.5 mL of HCl, 2.5 mL of HNO_3, and 95 mL of H_2O. The microstructures of the welds were observed by using an Inspect F50 field-emission scanning electron microscopy (FE-SEM) system (Thermo Fisher Scientific, Waltham, MA, USA) in combination with a Pegasus Hikari electron backscatter diffraction (EBSD) analysis system (EBSD-EDAX, AMETEK, Berwyn, PA, USA). The EBSD specimens were mechanically polished and then electropolished at room temperature in a solution of 10% perchloric acid and ethanol under the condition of an operating voltage of 17 V. The critical misorientation angle was set to be 15° for grain identification. The data were interpreted by using orientation imaging microscopy analysis software (OIM v6.2, EDAX Inc., Mahwah, NJ, USA).

3. Results & Discussion

3.1. Asymmetric and Symmetric Pulses in Arc Power Source

The CMT advanced power source (Frounius, Wels, Austria) provided a synergic line that controlled the polarity, current, time, and rise rate to optimize work performance and convenience. These waveforms (synergic lines) were generally designed to be asymmetric with respect to the current and duration of the phases to maintain the arc stability and periodic droplet transfer. The waveform obtained by applying the synergic line of AlMg5 is shown in Figure 4. The peak current and duration of the EN phase were lower and shorter, respectively, than those of the EP phase. This indicates that the heat input per EP mode pulse is different from that per EN mode pulse. In addition, it can be inferred from these results that the effects of EN pulses and their repetitions on the microstructural growth and geometrical features of WAAM have not been clearly analyzed in the previous studies.
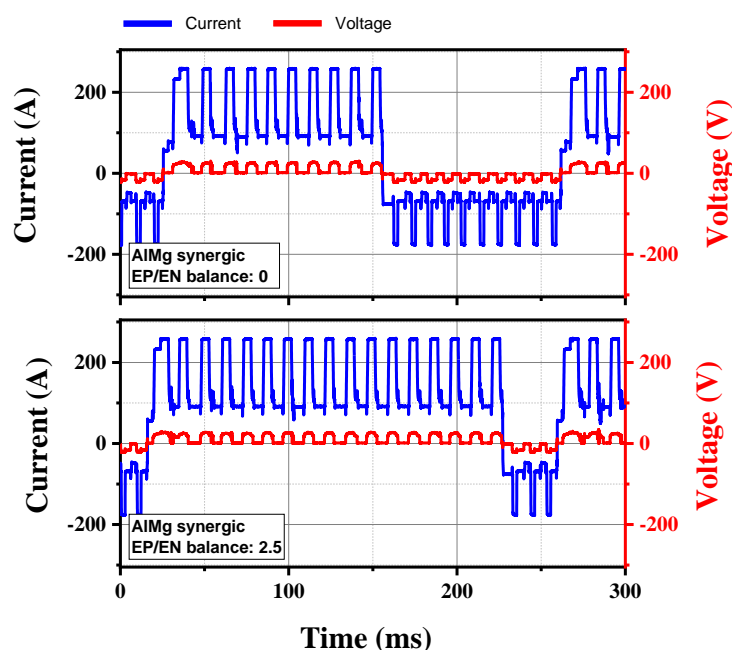

Figure 4. Measured waveform utilizing AlMg5 synergic line.

In addition, the application of EP/EN balance factor, which is a control parameter of CMT power source, complicates the analysis of the experimental results. Although applying EP/EN balance factor facilitates easy manipulation of the phase distribution, it is difficult to intuitively understand because it does not have a linear tendency. As shown in Figure 5, the R_{EN} utilized in this study was expressed as a linear line; additionally, the EP/EN balance of the aluminum synergic lines was recalculated; the results are presented as dots in the figure. In the case of the AlSi5 synergic line, the deviation of the R_{EN} and EP/EN balance increased up to ± 2 of the EP/EN balance, and then decreased. Because

each synergic line was associated with different numbers of EN pulses in a single cycle (Table 4), it was not appropriate to conduct an experiment with the EP/EN balance factor as a parameter.
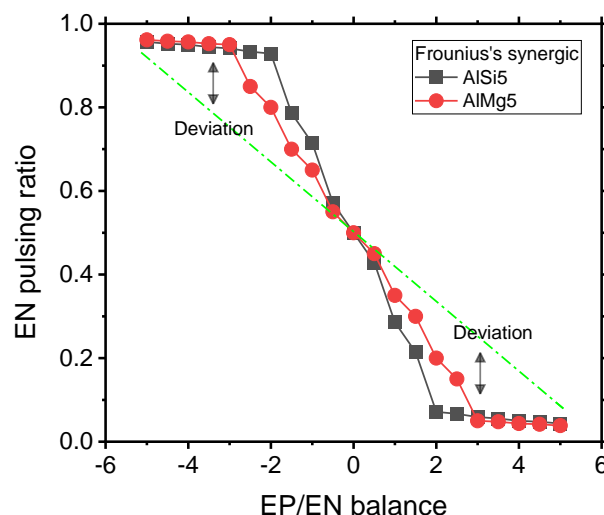

**Figure 5.** Relationship between the EP/EN balance and EN pulsing ratio.

Table 4. EP/EN balance and recalculated EN pulsing ratio values for the AlSi5 and AlMg5 synergic line.

| EP/EN Balance	−4.0		−1.5		0.0		1.5		4.0	
	AlSi5	AlMg5	AlSi5	AlMg5	AlSi5	AlMg5	AlSi5	AlMg5	AlSi5	AlMg5
EN pulses in a cycle	1	1	3	6	7	10	11	14	19	22
EP pulses in a cycle	19	22	11	14	7	10	3	6	1	1
Recalculated EN pulsing ratio	**0.95**	**0.96**	**0.79**	**0.7**	**0.5**	**0.5**	**0.21**	**0.3**	**0.05**	**0.04**

Note: EN pulsing ratio = Number of EN pulses/Total pulses in one cycle (EN + EP pulses).

The current parameters were manually tuned to obtain a symmetric pulse sequence and power supply. The data acquisition system was used to acquire the current waveforms according to the R_{EN}; the results are presented in Figure 6. The peak, base, detach current, and duration were symmetrically organized, and the symmetricity was found to be better when the same phases were repeated within a cycle; this was also true under high repetition conditions. This is attributable to the temporary increase in the base current after the polarity change. Consequently, it was possible to use a manual tuning method to implement a symmetrical pulse sequence. Figure 7a–c shows the power, current, and voltage values according to the R_{EN} under different welding speed conditions. These values were characterized as root-mean-square (RMS) to ignore time-varying periodic voltage and current. The current and power were similar up to an R_{EN} of 0.5, and then began to slightly decrease with increasing R_{EN}. The lowest power was induced when R_{EN} was 1. The dependence of voltage on the welding speed and R_{EN} was insignificant as compared to the current and power (Figure 7b). Furthermore, relatively lower power values were measured under the relatively higher repetition conditions (Figure 7d). The differences in power between the relatively high and low repetition conditions increased in magnitude until R_{EN} was increased to 0.5, beyond which value the magnitude of the differences began to decrease. It can be inferred from these results that frequent polarity changes affected the waveform and amount of supplied power.
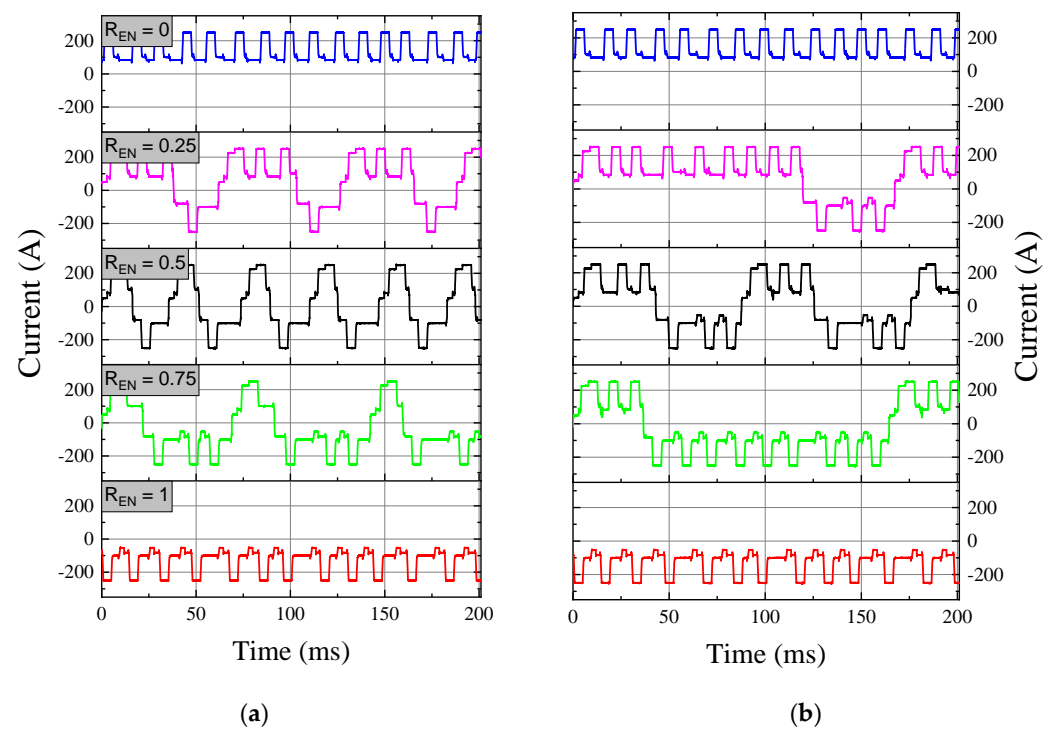
Figure 6. Current waveforms acquired under the conditions of (**a**) one and (**b**) three pulse repetitions at welding speed of 0.7 m/min.
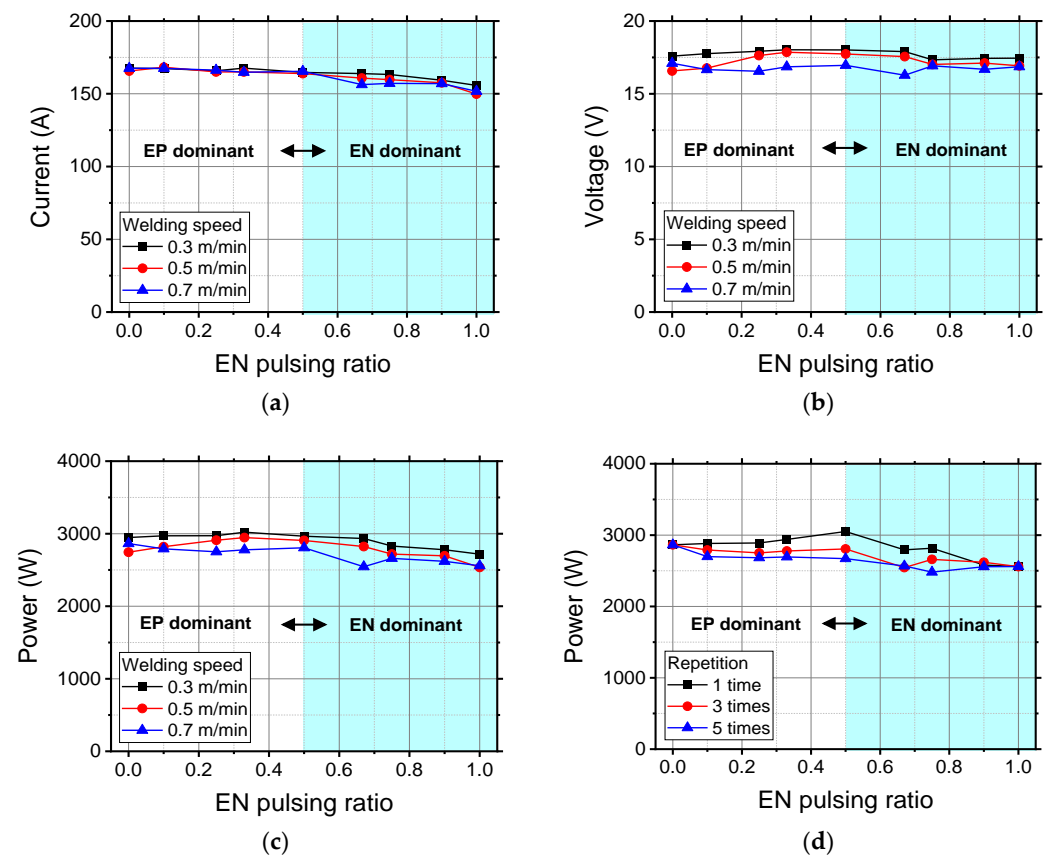
Figure 7. (**a**) RMS current, (**b**) voltage, and (**c**) supplied power for different welding speeds and R_{EN} values; (**d**) supplied power R_{EN} measured under different repetition and R_{EN} conditions. The welding speed was 0.7 m/min.

3.2. Droplet Transfer and Arc Behavior According to Polarity

The arc concentration and droplet behavior were found to be dependent on polarity. As shown in Figure 8, a longer arc length was observed during the EP phase because of the change in electron movement. The electrons moved from the surface of the substrate to the filler wire during the EP phase, whereas the electrons were transmitted from the surface of the wire to the substrate during the EN phase.


| (**a**) EP-base | (**b**) EP-peak | (**c**) EP-detach |
| (**d**) EN-base | (**e**) EN-peak | (**f**) EN-detach |
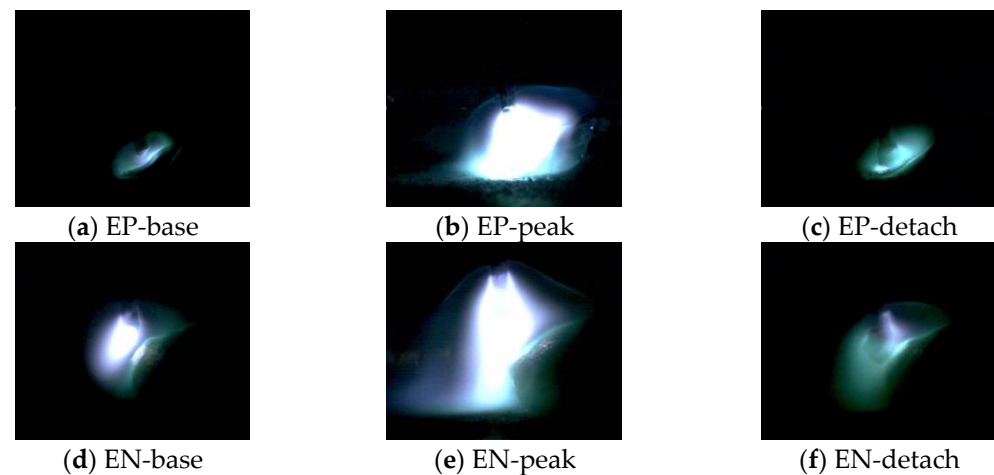
Figure 8. Arc length observations: (**a**–**c**) EP subphases, and (**d**–**f**) EN subphases.

The application of the VP-CMT power source in the WAAM process resulted in the generation of stable arcs and periodic droplet transfers regardless of the R_{EN}. Figure 9 shows the images captured by the high-speed camera before the droplets made contact with the molten pool. The droplets formed during the peak current period were transferred to the molten pool via the push-pull motion of the welding torch during the detachment period. Furthermore, the droplets that were delivered during the EP phase (Figure 9i–v) were smaller than those delivered during the EN phase (Figure 9vi–x). As the R_{EN} approached 0.5, the polarity changed frequently, and the droplet transfer was reduced because of the longer duration of the base current (IB_EP or IB_EN), which was required to maintain arc stability after polarity switching. As shown in Figure 6a, eleven droplet transfers occurred within a period of 200 ms under the conditions of an R_{EN} value of 0.5. Under the conditions of R_{EN} values of 0 and 1, the droplets were transferred 15 and 13 times, respectively.

The polarity and repetition were found to affect the behavior of the molten pool. The short and strong arc generated during the EP phase (Figure 9i–v) had a stronger compression effect on the molten pool surface than the arc generated during the EN phase (Figure 9vi–x). An increase in the strength of this compression effect was also observed with increasing EP pulse repetition; alternatively, increasing the EN pulse repetition corresponded to the accumulation of molten metal below the filler wire. Consequently, and as reported by Babu et al., the molten pool surface periodically varied depending on the polarity switching [23]. As the number of repetitions increased, the dependence of the droplet transfer on the R_{EN} decreased. In the case of three repetitions (Figure 6b), more droplet transfers occurred within the same period compared to one repetition. This means that designing the WAAM process to prevent frequent polarity changes would be beneficial for the stacking materials.
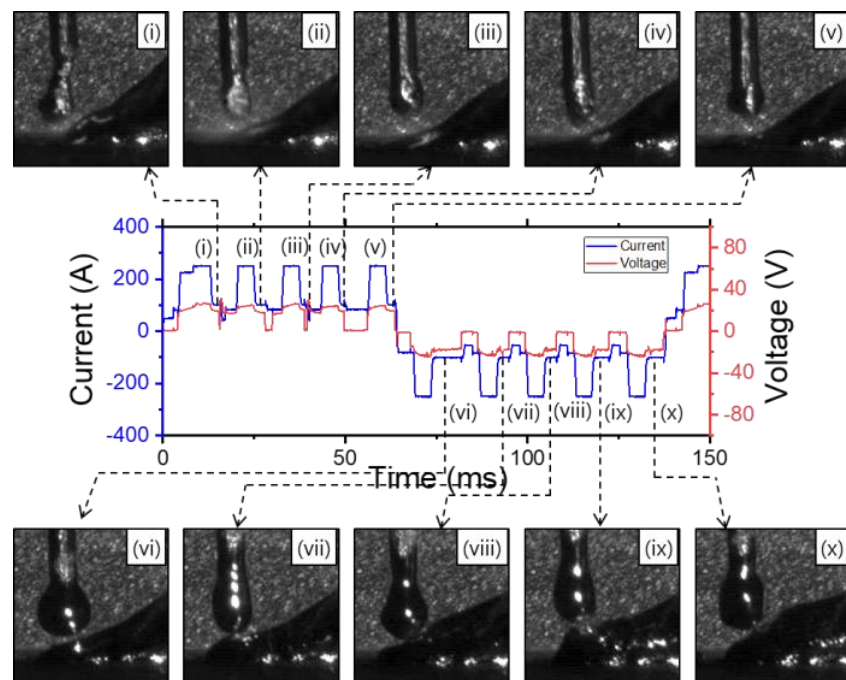
Figure 9. Observation of droplet transfer and molten pool deformation throughout the EP (**i–v**) and EN (**vi–x**) phases. The images were captured under the conditions of a welding speed of 0.3 m/min, five pulse repetitions, and an R_{EN} of 0.5.

3.3. Geometrical Characteristics of Deposited Metal

Polarity switching and its frequency are known to affect the final characteristics of the deposited materials, such as the surface roughness and wetting angle. Figure 10 shows the bead appearance and macro images of the welds produced under the conditions of different R_{EN} and repetition. Under the condition of three repetitions (Figure 10c–g), an unstable arc and non-uniform bead appearance were observed (Figure 10g) at higher R_{EN} values. Additionally, ripple was clearly observed in the cases of three and five repetitions (Figure 10c–i), although it was not observed in the case of one repetition (Figure 10a,b).

| R_{EN}	Bead appearance	Macro image
Repetition 1		
(**a**) 0.25		
(**b**) 0.75		
Repetition 3		

Figure 10. *Cont.*
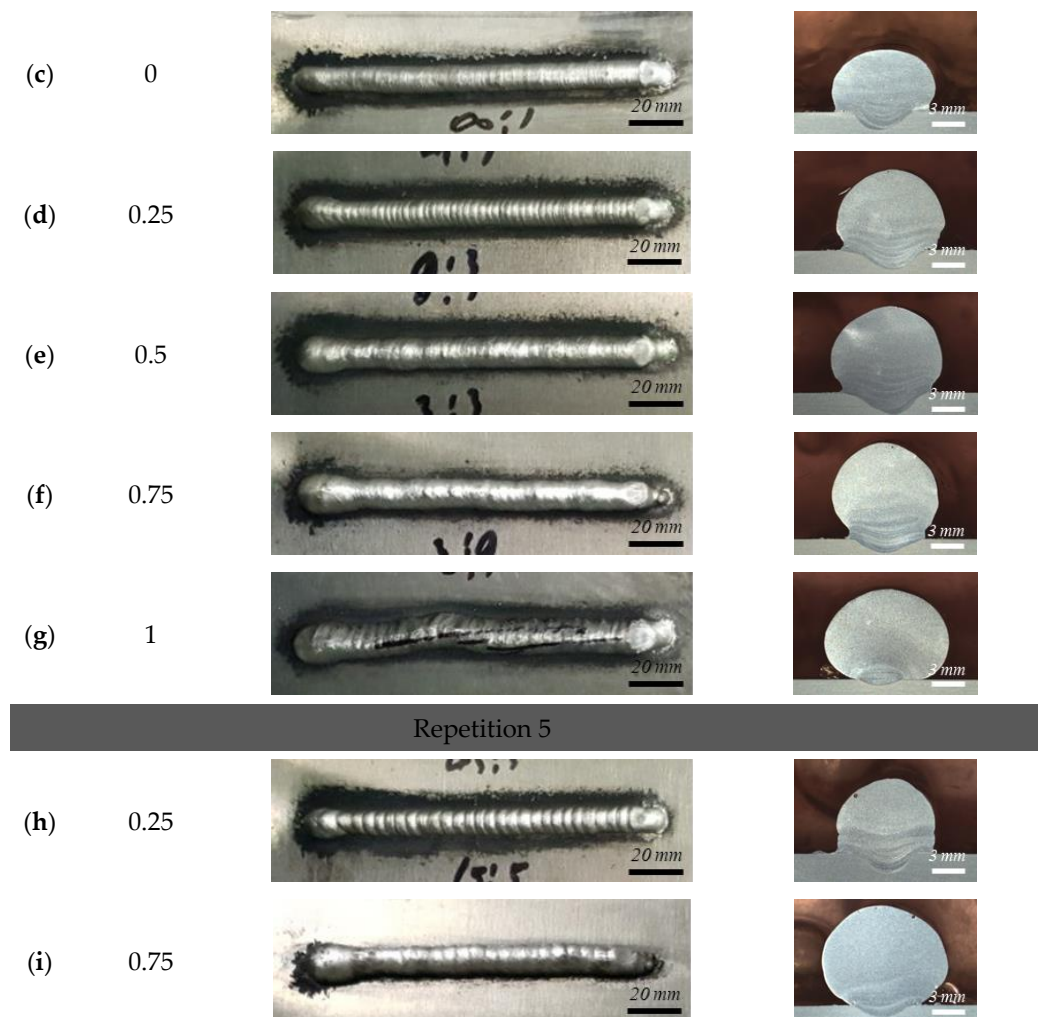
Figure 10. Bead appearance and cross-sectional images depending on R_{EN} and repetition conditions. Specimens were fabricated at a welding speed of 0.5 m/min.

The R_{EN} value was found to not only influence the bead width and height, but also the deposition area and substrate dilution (Figure 11). The bead width, bead height, deposition area, and dilution area are shown in Figure 11a. As the R_{EN} value increased, the height and width of the beads tended to increase. Additionally, the bead height and width were larger at low welding speeds than at high welding speeds (Figure 11b). The deposition area also increased as R_{EN} increased, whereas the deposition and dilution area tended to decrease under EN phase-dominant conditions (i.e., >0.5 R_{EN}), as shown in Figure 11c,d. When the EP phase was dominant (<0.5 R_{EN}), there was insignificant change in the dilution area; alternatively, the dilution area rapidly decreased under EN phase-dominant conditions (>0.5 R_{EN}). The weight of the deposited material at a length of 120 mm was measured under the conditions of different R_{EN} values and welding velocities (Figure 12a). The weight tended to increase with decreasing welding speed and increasing R_{EN}. The deposition weight of a zero R_{EN} value (only EP) was measured to be less than 50% of the weight of a one R_{EN} value (only EN). As the R_{EN} value increased, the amount of power required for the deposited metal decreased (Figure 12b). This indicates that the energy efficiency could be increased by adjusting the EN pulses.
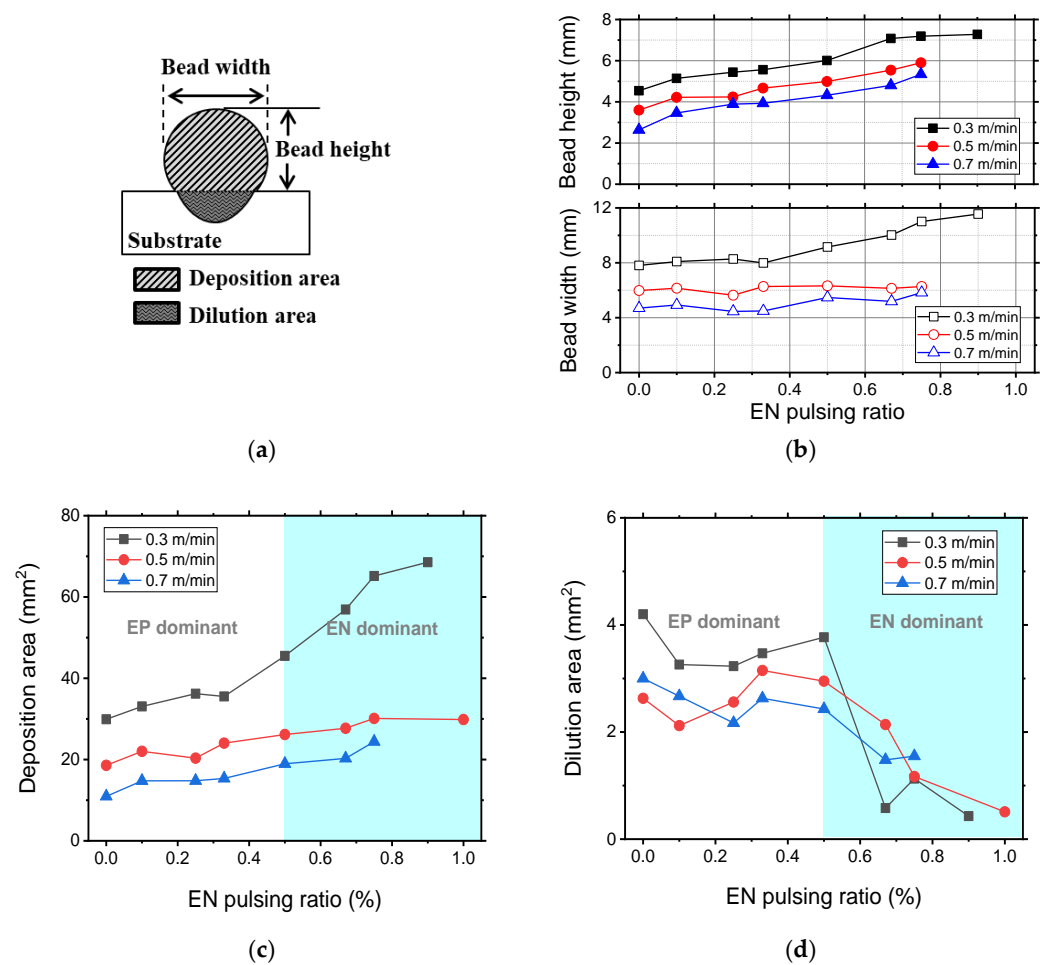
Figure 11. (**a**) Definition of geometrical factors that were analyzed according to the EN pulsing ratio; (**b**) bead height and width results; (**c**) deposition area results; and (**d**) dilution area results. These results were obtained for specimens that were measured under the three-repetition condition.
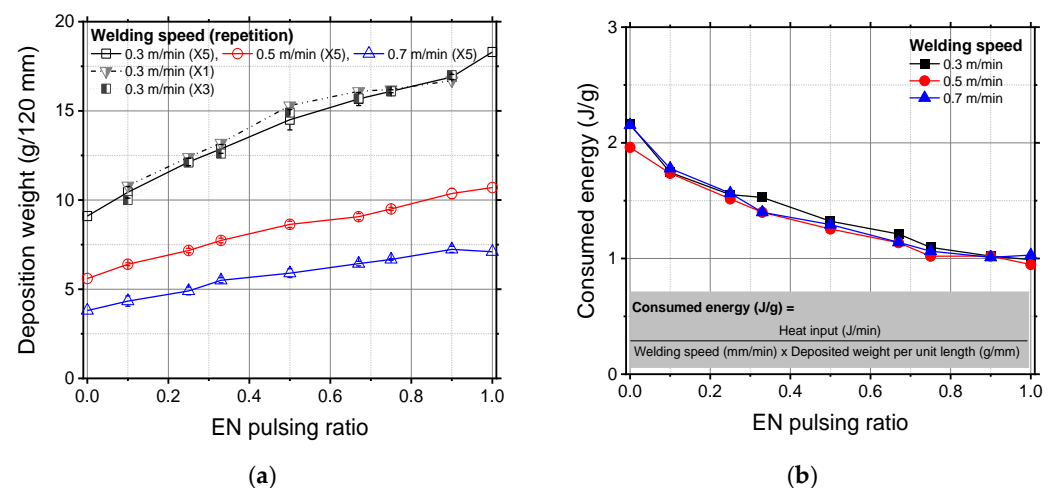
Figure 12. (**a**) Weight of deposited materials per 120 mm of weld length and (**b**) amount of energy consumed by additive deposition process as functions of the EN pulsing ratio.

The height and width largely varied under high repetition conditions, since repetition promoted ripple formation. The influence of the number of repetitions on the weight was not particularly strong, but the strongest influence was observed under the condition of R_{EN} = 0.5, which was also associated with frequent polarity switching (Figure 12a). These

results indicate that, under the conditions of WAAM using a VP-CMT power source, the droplet transfer can be regulated by adjusting the R_{EN} value and number of repetitions.

### 3.4. Dependency of Microstructural Formation of Deposited Metal

The mechanism of microstructure formation that occurs during the VP-GMAW-based WAAM process is complex because of the inherent characteristics of polarity switching. Microstructural growth can be affected by numerous factors, such as chemical composition, impurities, and welding parameters. Typically, it is largely determined by the cooling rate and heat input. At a fast cooling rate and under low heat input conditions, a finer structure can be formed. Klein and Schnall [10] insisted that heat input conditions significantly influence grain size, as it is determined by the maximum temperature and cooling rate. In general, fine grains are formed under conditions of low heat input and high welding speed. For instance, a fast solidification rate and small temperature gradient were found to result in an equiaxed structure. In addition, Zhang et al. [20] explained that, under the conditions of implementation of VP-CMT in the WAAM process, the generated magnetic field was periodically reversed, and that this resulted in intense convection in the molten pool. The authors suggested that the convection broke the dendrite arms and formed small nuclei. Additionally, according to Babu et al. [23], the periodic variation in the molten pool shape and periodic interruptions in the growth process may have significantly contributed to the refinement of the grain structure. Sundaresan et al. [24] also reported that current pulsing enhanced the molten pool fluid flow and reduced the temperature gradient, which was induced by the continuous changes in the molten pool size and shape.

As previously mentioned, the R_{EN} value and number of repetitions affected dilution and penetration behaviors, ultimately creating a difference in the chemical composition and thermal history of the welds. The formation of the equiaxed structure was dominant in all samples, except when the degree of substrate dilution was higher (i.e., at lower R_{EN} values). The influence of R_{EN} on the microstructure was visualized by generating the inverse pole figure map shown in Figure 13. As can be seen, as the R_{EN} value increased, the penetration depth increased, and the fraction of columnar structures in the welds increased. Rapid heat loss via conduction caused the columnar structures, which are indicated by yellow arrows in Figure 13a, to be readily generated at the fusion boundary, which was in contact with the substrate. The average grain sizes, marked in Figure 13a–c, were analyzed to be 67.3, 55.6, and 78.0 μm. The largest grain was obtained when minimum power supplied condition, $R_{EN} = 1$. Grain size was also associated with frequent polarity switching. Grain size decreased as the frequency of polarity switch increased. Finer grains were found under high repetition conditions as shown in Figure 14. The grain sizes were analyzed to be 59.9, 57.9, and 52.7 μm as the repetitions continued to increase. Based on these results, the average grain size is believed to be related to the amount of supplied power, as well as the polarity switching that occurs during grain formation.

Average grain size: 67.3 μm	Average grain size: 55.6 μm	Average grain size: 78.0 μm
(a)	(b)	(c)
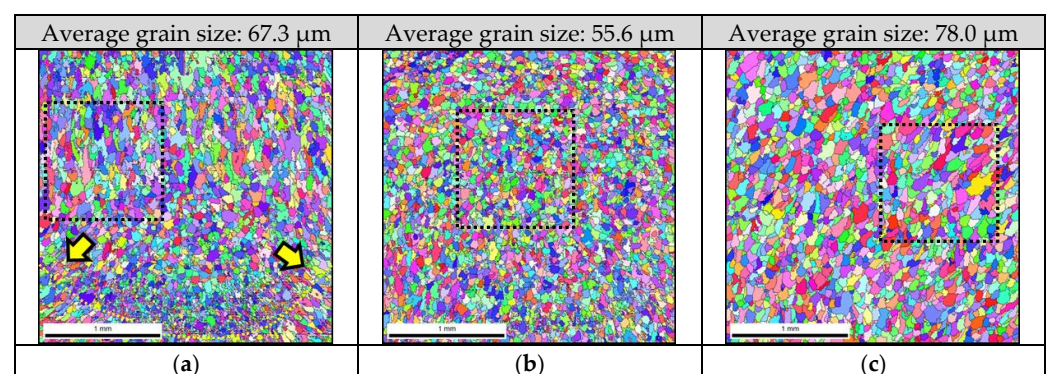
Figure 13. EBSD results for (**a**) $R_{EN} = 0$, (**b**) $R_{EN} = 0.25$, and (**c**) $R_{EN} = 1$. The specimens were prepared under the conditions of a welding speed of 0.5 m/min and one repetition.

Average grain size: 59.9 μm	Average grain size: 57.9 μm	Average grain size: 52.7 μm
(**a**)	(**b**)	(**c**)
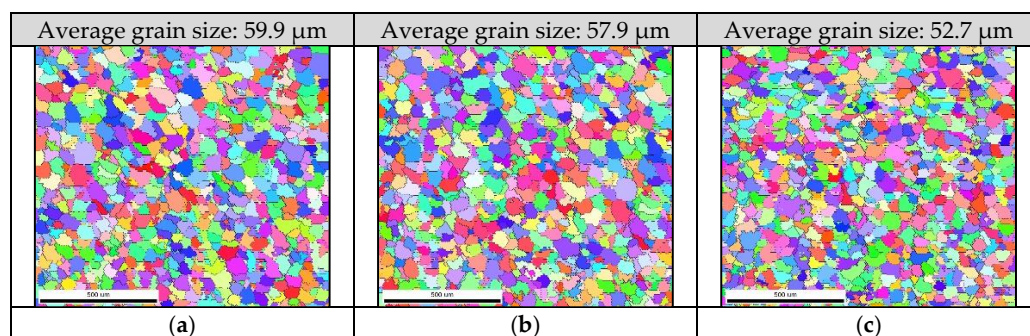
Figure 14. EBSD results for (**a**) one, (**b**) three, and (**c**) five repetitions. The specimens were prepared at a welding speed of 0.5 m/min and R_{EN} of 0.5. Scale bar = 500 μm.

VP-GMAW has significant potential as an additive manufacturing technique for aluminum because EN pulsing can increase the rate of deposition and enhance the equiaxed microstructure. Thus, when VP-GMAW is applied to the WAAM process, it can be considered advantageous as a tool to ensure adequate levels of productivity. Although the application of a relatively high R_{EN} value and high repetition were beneficial from the perspective of grain refinement, it resulted in the formation of ripples. Thus, an EN pulsing ratio of 0.5–0.7 and fewer repetitions are recommended when applying WAAM to aluminum alloys.

4. Conclusions

In this study, VP-GMAW-based WAAM was performed, and the effects of the EN pulsing ratio and pulse repetition on the geometrical and morphological characteristics were investigated. Additionally, the current and voltage were analyzed with respect to the EN pulsing ratio to verify process stability. The following conclusions were drawn.

(1) The waveforms were manually tuned to obtain a symmetrical pulse sequence. The peak, base, detach current, and time were well suited for additive manufacturing. The waveform was found to have high symmetry under the same pulse repetition condition.

(2) The polarity and its repetition were found to affect the droplet transfer and molten pool behavior. Under the condition of frequent polarity switching, droplet transfer was reduced because the duration of the base current subphase (after polarity switching) was relatively longer. In addition, the molten pool surface periodically deformed depending on the polarity. The short and strong arc that was generated during the EP phase effectively compressed the molten pool surface; alternatively, the droplets accumulated below the wire during the EN phase.

(3) Polarity switching and the frequency at which it occurred affected the final feature of the WAAM product. Additionally, R_{EN} was found to not only influence the bead width and height, but also the deposition area and substrate dilution. When an R_{EN} was zero, the weight of the deposited material was found to be less than 50% of the weight of one R_{EN}. Increasing the number of repetitions was found to increase the roughness of height and width.

(4) The grain size is believed to be related to the amount of supplied power, as well as the polarity switching frequency. The generation of an equiaxed structure occurred in all samples. As the penetration depth increased, the R_{EN} value was low, and the rapid heat loss via conduction caused the fraction of columnar structures in the weld to increased. The columnar microstructure formed at the interface might cause structural anisotropy of the product. Therefore, it was recommended to select a relatively high EN pulse rate, where the equiaxed structure was dominant and the deposition amount was high.

Institutional Review Board Statement: Not applicable.

Informed Consent Statement: Not applicable.

Data Availability Statement: Not applicable.

Conflicts of Interest: The authors declare no conflict of interest.

References

1. Ding, D.; Pan, Z.; Cuiuri, D.; Li, H. A multi-bead overlapping model for robotic wire and arc additive manufacturing (WAAM). *Robot. Comput. Integr. Manuf.* **2015**, *31*, 101–110. [CrossRef]
2. Shamsaei, N.; Yadollahi, A.; Bian, L.; Thompson, S.M. An overview of direct laser deposition for additive manufacturing; Part II: Mechanical behavior, process parameter optimization and control. *Addit. Manuf.* **2015**, *8*, 12–35. [CrossRef]
3. Thompson, S.M.; Bian, L.; Shamsaei, N.; Yadollahi, A. An overview of direct laser deposition for additive manufacturing; Part I: Transport phenomena, modeling and diagnostics. *Addit. Manuf.* **2015**, *8*, 36–62. [CrossRef]
4. Wanjara, P.; Brochu, M.; Jahazi, M. Electron beam freeforming of stainless steel using solid wire feed. *Mater. Des.* **2007**, *28*, 2278–2286. [CrossRef]
5. Mazumder, J.; Dutta, D.; Kikuchi, N.; Ghosh, A. Closed loop direct metal deposition: Art to part. *Opt. Lasers Eng.* **2000**, *34*, 397–414. [CrossRef]
6. Frazier, W.E. Metal additive manufacturing: A review. *J. Mater. Eng. Perform.* **2014**, *23*, 1917–1928. [CrossRef]
7. Popov, V.V.; Fleisher, A. Hybrid additive manufacturing of steels and alloys. *Manuf. Rev.* **2020**, *7*, 1–9. [CrossRef]
8. Cunningham, C.R.; Flynn, J.M.; Shokrani, A.; Dhokia, V.; Newman, S.T. Invited review article: Strategies and processes for high quality wire arc additive manufacturing. *Addit. Manuf.* **2018**, *22*, 672–686. [CrossRef]
9. Ding, D.; Pan, Z.; Cuiuri, D.; Li, H. Wire-feed additive manufacturing of metal components: Technologies, developments and future interests. *Int. J. Adv. Manuf. Technol.* **2015**, *81*, 465–481. [CrossRef]
10. Klein, T.; Schnall, M. Control of macro-/microstructure and mechanical properties of a wire-arc additive manufactured aluminum alloy. *Int. J. Adv. Manuf. Technol.* **2020**, *108*, 235–244. [CrossRef]
11. Hu, Y.Y.; Mu, S.; Wang, J. Arc Behavior and Droplet Transfer Process of VP CMT. *Appl. Mech. Mater.* **2014**, *467*, 81–85. [CrossRef]
12. Kiran, D.V.; Cheon, J.; Arif, N.; Chung, H.; Na, S.-J. Three-dimensional finite element modeling of pulsed AC gas metal arc welding process. *Int. J. Adv. Manuf. Technol.* **2016**, *86*, 1453–1474. [CrossRef]
13. Wang, H.; Kovacevic, R. Rapid prototyping based on variable polarity gas tungsten arc welding for a 5356-aluminium alloy. *Proc. Inst. Mech. Eng. B J. Eng. Manuf.* **2001**, *215*, 1519–1527. [CrossRef]
14. Harwig, D.; Dierksheide, J.; Yapp, D.; Blackman, S. Arc behavior and melting rate in the VP-GMAW process. *Weld. J.* **2006**, *85*, 52–62.
15. Park, H.J.; Kim, D.C.; Kang, M.J.; Rhee, S. The arc phenomenon by the characteristic of EN ratio in AC pulse GMAW. *Int. J. Adv. Manuf. Technol.* **2013**, *66*, 867–875. [CrossRef]
16. Su, C.; Chen, X.; Gao, C.; Wang, Y. Effect of heat input on microstructure and mechanical properties of Al-Mg alloys fabricated by WAAM. *Appl. Surf. Sci.* **2019**, *486*, 431–440. [CrossRef]
17. Cong, B.; Ding, J.; Williams, S. Effect of arc mode in cold metal transfer process on porosity of additively manufactured Al-6.3%Cu alloy. *Int. J. Adv. Manuf. Technol.* **2015**, *76*, 1593–1606. [CrossRef]
18. Cong, B.; Qi, Z.; Qi, B.; Sun, H.; Zhao, G.; Ding, J. A comparative study of additively manufactured thin wall and block structure with Al-6.3% Cu alloy using cold metal transfer process. *Appl. Sci.* **2017**, *7*, 275. [CrossRef]
19. Baoqiang, C.; Ruijie, O.; Bojin, Q.; Jialuo, D. Influence of cold metal transfer process and its heat input on weld bead geometry and porosity of aluminum-copper alloy welds. *Rare Met. Mater. Eng.* **2016**, *45*, 606–611. [CrossRef]
20. Zhang, B.; Wang, C.; Wang, Z.; Zhang, L.; Gao, Q. Microstructure and properties of Al alloy ER5183 deposited by variable polarity cold metal transfer. *J. Mater. Process. Technol.* **2019**, *267*, 167–176. [CrossRef]
21. Zhang, C.; Gao, M.; Zeng, X. Workpiece vibration augmented wire arc additive manufacturing of high strength aluminum alloy. *J. Mater. Process. Technol.* **2019**, *271*, 85–92. [CrossRef]
22. Zhang, C.; Li, Y.; Gao, M.; Zeng, X. Wire arc additive manufacturing of Al-6Mg alloy using variable polarity cold metal transfer arc as power source. *Mater. Sci. Eng. A* **2018**, *711*, 415–423. [CrossRef]

23. Babu, N.K.; Raman, S.G.S.; Mythili, R.; Saroja, S. Correlation of microstructure with mechanical properties of TIG weldments of Ti–6Al–4V made with and without current pulsing. *Mater. Charact.* **2007**, *58*, 581–587. [CrossRef]

24. Sundaresan, S.; Ram, G.D.J.; Reddy, G.M. Microstructural refinement of weld fusion zones in α–β titanium alloys using pulsed current welding. *Mater. Sci. Eng. A* **1999**, *262*, 88–100. [CrossRef]